Supporting Information

Highly Chemoresistive Humidity Sensing using Poly(ionic liquid)s

Lingling Wang, Xiaochuan Duan*, Wuyuan Xie, Qiuhong Li* and Taihong Wang

Experimental section

Materials:

1-vinyl-3-ethylimidazolium bromide was obtained from Lanzhou Greenchem ILS, LICP. CAS. China. 2, 2'-Azobis (2-methylpropionitrile) (AIBN), sodium tetrafluoroborate ($NaBF_4$) and other chemicals were purchased from Sigma-Aldrich Company and used as received without further purifications. The water used was deionized.

Synthesis of Poly(1-ethyl-3-vinylimidazolium bromide):

In a typical synthesis process, 10.38 g of 1-vinyl-3-ethylimidazolium bromide, 30 mg of AIBN and 70 mL absolute ethanol were added into a 250 mL of round-bottom flask. The mixture solution was stirred for 2 h with nitrogen to remove oxygen, and then heated to 70 ^oC for 24 h.[1] After that, the Poly(1-ethyl-3-vinylimidazolium bromide) (PEVIm-Br) was washed with tetrahydrofuran (THF) and then dried at 70 ^oC overnight. The schematic diagram is as follows:

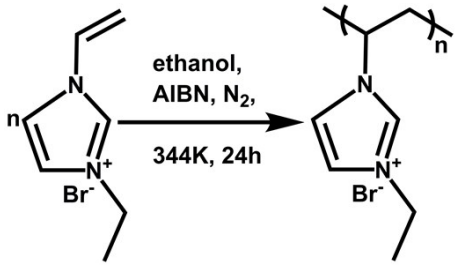

Synthesis of Poly(1-ethyl-3-vinylimidazolium tetrafluoroborate):

In a typical synthesis process, 2.04 g of PEVIm-Br was dissolved in 9 mL of deionized water and 9 mL of absolute ethanol (solution A) under magnetic stirring in ice-water bath for 30 minutes. Meanwhile, 1.098 g of $NaBF_4$ was dissolved in 9 mL of deionized water and 9 mL of absolute ethanol (solution B) under magnetic stirring in ice-water bath for 30 minutes. Subsequently, the solution B was slowly added into solution A, the mixture was stirred in ice-water bath for 30 minutes and then stand for 1 hour. The resulting yellowish white solid was cleaned with deionized

water and absolute ethanol several times and dried at 70 °C for 24 hours.[2]. The schematic diagram is as follows:

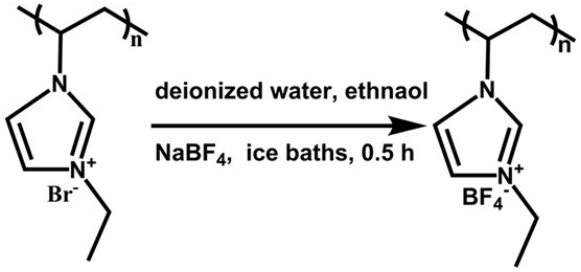

Preparation of humidity sensor and testing instrumentation:

The sensors were fabricated by spin-coating the PEVIm-Br dispersion onto the pre-cleaned interdigitated electrodes. Alumina ceramic was used as the substrate due to its high dielectric strength and excellent chemical stability. The interdigitated electrodes composed of 10 nm of titanium and 80 nm of gold with a line width of 80 μm, were fabricated by sputtering as shown in Figure S1.

Spin-coating PEVIm-Br onto the interdigitated electrodes: 0.16 g of PEVIm-Br was added into 0.374 g of absolute ethanol and the mixture solution was stirred for 2 hours to be completely dissolved. The sensors were fabricated by spinning 2.5 μL mixture solutions onto the pre-cleaned interdigitated electrodes at the speed of 4000 rad/s for 60 s. And then the sensor was dried at room temperature for 48 h. For the case of PEVIm-BF_4, the solution was replaced by dimethyl formamide (DMF) with other conditions preserved the same. The thickness of PEVIm-Br can be easily tuned by adjusting the solution concentration and revolving speed (Table S1).

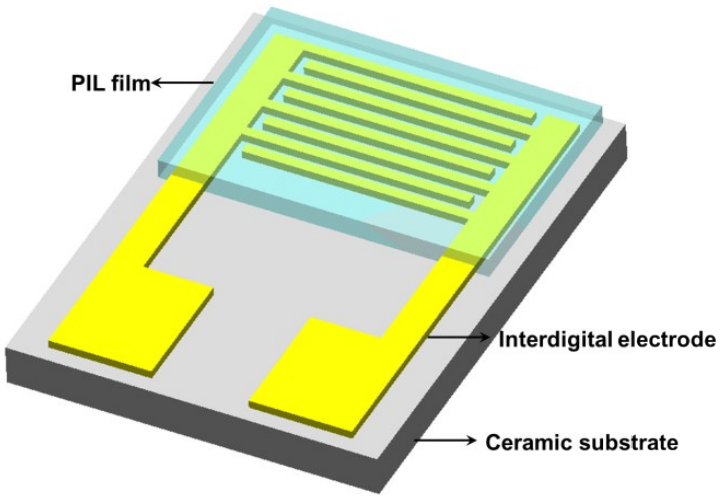

Figure S1. Schematic diagram of PIL-based humidity sensor.

Table S1. Parameters of spin-coating and their corresponding thickness of PEVIm-Br film

Solution concentration (%)	Revolving speed (rad/s)	Thickness (μm)
5	6000	1.5
10	6000	4.7
5	4000	16.7
15	4000	30
30	4000	62
30	2000	72
30	1000	96

Humidity sensing properties were tested by an impedance analyzer (Agilent 4294, 40 Hz to 100 MHz). The applied voltage amplitude was of 500 mV, and the measuring temperature was about 25 °C. Several 250 mL bottles containing different saturated salt solutions including LiCl, $MgCl_2$, K_2CO_3, NaBr, NaCl, KCl, and K_2SO_4were used as the humidity sources of 11%, 33%, 43%, 59%, 75%, 85% and 98% RH, respectively.

Characterization of Poly(ionic liquid)s:

Elemental analysis of PEVIm-Br and PEVIm-BF_4.

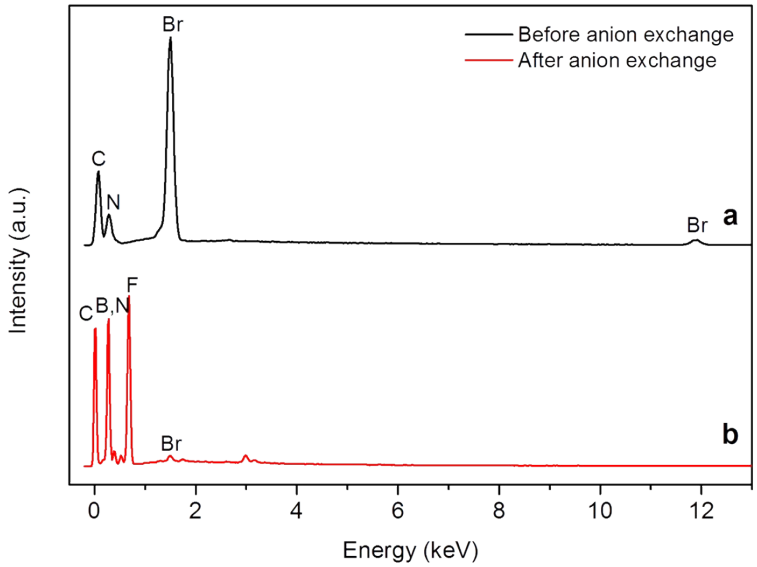

Figure S2. Energy-dispersive X-ray spectrums of (a) PEVIm-Br, before anion exchange; and (b) PEVIm-BF_4, after anion exchange.

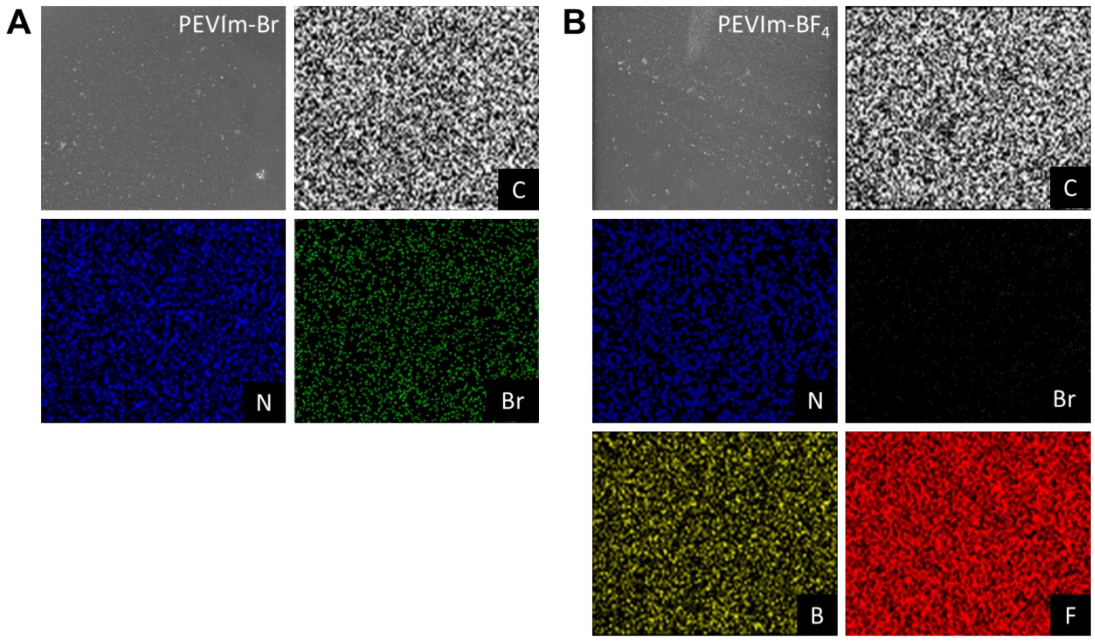

Figure S3. SEM image and corresponding elemental mappings of (A) PEVIm-Br, before anion exchange; and (B) PEVIm-BF_4, after anion exchange.

Fourier transform infrared (FTIR) spectrogram was performed on a Thermo Nicolet 330 in the range of 400-4000 cm^{-1}. The FTIR spectrogram of PEVIm-Br and PEVIm-BF_4 were shown in Figure S2. The transmittance peak assigned to imidazole ring was clear, the absorption peaks near 1572, 3132 cm^{-1} was due to the stretching vibration of C=N and C-H bond of imidazole ring, the band at 1170 cm^{-1} resulted from the in-plane deformation vibrations of C-H of imidazole ring, and the out-of-plane bending vibration of C-H of imidazole ring was observed at 760 and 650 cm^{-1}. The broad absorption peak around 3450 cm^{-1} was attributed to O-H of physical adsorbed water.[3] The corresponding peak of BF_4^- was observed at 1058 cm^{-1}.

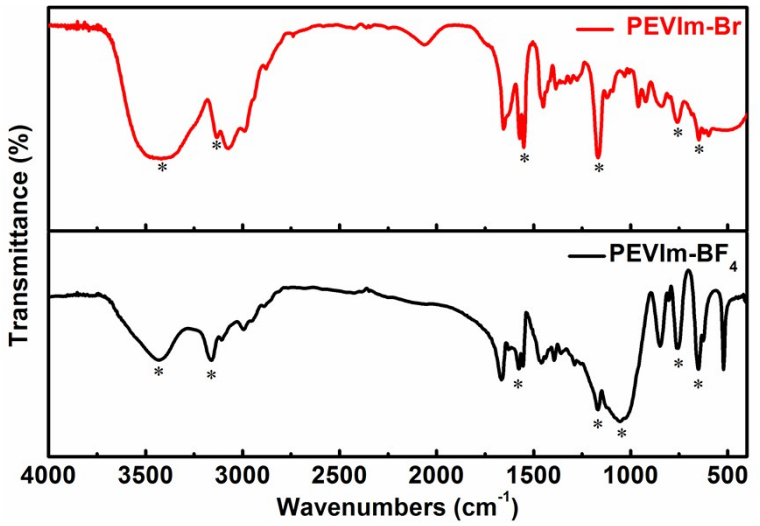

Figure S4. FTIR spectrograms of PEVIm-Br and PEVIm-BF_4.

Proton nuclear magnetic resonance (1H-NMR) spectrum was tested by Bruker Advance II400 MHz and shown in Figure S3. 1H-NMR (THF), δ(ppm)： 7.53(c and d, C-H), 4.15(e, C-H; b, C-H_2), 2.45(f, C-H_2), 1.42(a, -CH_3). The disappearance of the vinyl signal at 5.67 ppm can be observed, indicating that the PEVIm-Br was synthesized by radical polymerization of ionic liquid monomers (VEIm-Br).

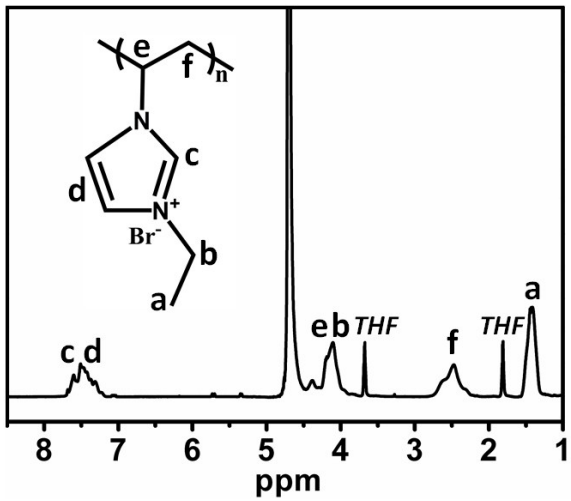

Figure S5 [1]H-NMR spectrum of PEVIm-Br.

Molecular Weight: The molecular weight of PEVIm-Br was analyzed by matrix-assisted laser desorption/ionization time of flight mass spectrometry (MALDT-TOF-MS). All mass spectra were obtained with a Microflex LRF MALDT-TOF-MS (Bruker Daltonics, Germany) and analyzed by flex analysis software provided by Bruker Daltonics Corp. MALDI source was equipped with a nitrogen laser (337 nm) for irradiation of analytes and an accelerating voltage from -20 kV to 20 kV was employed. For MALDI-TOF sample, the matrix solution was obtained by dispersing 1 mg of as-prepared PEVIm-Br in 3 mL of ultrapure water. The mixture of 5 μL of the above solution and 5μL of analyte solution (2,5-dihydroxybenzoic acid, DHB) was vortexed for 40 s, followed by directly doting 1μL of the matrix-analyte mixture onto the MALDI plate and dried in air for MALDI-TOF-MS analysis.

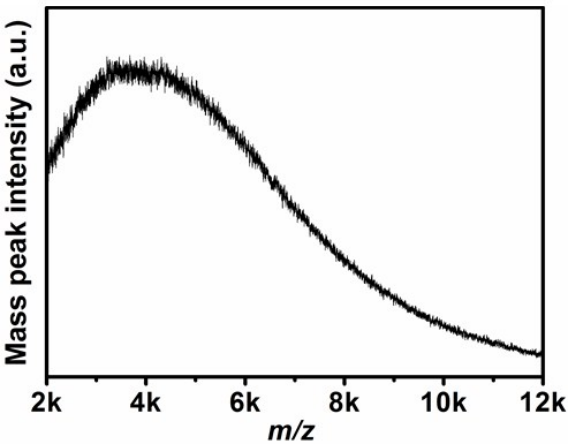

Figure S6. MALDT-TOF-MS of the as-prepared PEVIm-Br. It can be seen that the distribution of molecular weight of PEVIm-Br is from 2000-7000 g/mol, with an average molecular weight of 4120 g/mol.

Viscosity: The viscosities of the 50% PVEIm-Br aqueous solution was measured using an NDJ-1 viscometer (Shanghai Shunyu Hengping Scientific Instruments Co., Ltd.) in the temperature range from 298.15 to 328.15 K. The temperature was controlled using a thermostatic bath. The time for attaining thermal equilibrium in the viscosity determination was 30 min. The values were recorded at a regular interval of 10 K. Each datum point of viscosity was the average value of three measurements. The results are displayed in Figure S5. Generally, significant decrease of viscosity (η) can be observed in ionic liquids as temperature increase. For the ionic liquids containing big

asymmetric cations with functional groups in the alkyl chains, the viscosity-temperature relationship obeys the Vogel-Tamman-Fulcher (VTF) equation: $\eta = \eta_0 e^{B/T-T_0}$, where η_0 (mPas), B (K) and T_0 (K) are constants.

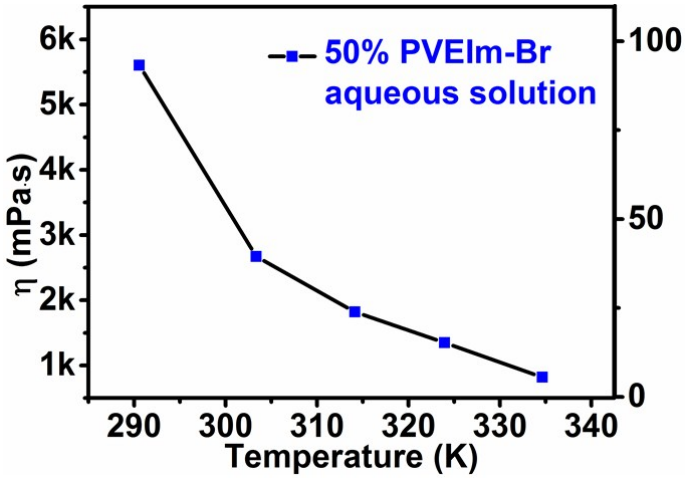

Figure S7. Temperature dependence of absolute viscosity of the 50 wt% PVEIm-Br aqueous solution.

Conductivity: The conductivity measurements of PVEIm-Br aqueous solutions were carried out on a DDSJ-318 conductivity instrument (Shanghai Electronics Science Instrument Co., Ltd. China) in the temperature range from 283.15 to 328.15 K. The temperature was controlled using a thermostatic bath. The time for attaining thermal equilibrium was 30 min. the values were recorded at interval of 10 K. ach datum point of conductivity was the average value of three measurements. The results are displayed in Figure S6. Generally, the content of water (or even trace levels of water) can significantly increases conductivity (κ) by lowering viscosity (η) in ionic liquid aqueous solution. The viscosity of ionic liquid aqueous solution is known to depend strongly on the content of water: the viscosity decreases rapidly as the content of water increases. According to the Walden Rule, the conductivity (κ) is inversely proportional to viscosity (η), thus the conductivity of 50 wt% PVEIm-Br aqueous solution is higher than 20 wt% PVEIm-Br aqueous solution. Besides, significant decrease of conductivity (κ) can be observed in both 20 wt% and 50 wt% PVEIm-Br aqueous solution as temperature increase, the conductivity-temperature relationship obeys the Vogel-Tamman-Fulcher (VTF) equation: $\kappa = \kappa_0 e^{-B/T-T_0}$, where κ_0 (mPas), B (K) and T_0 (K) are constants.

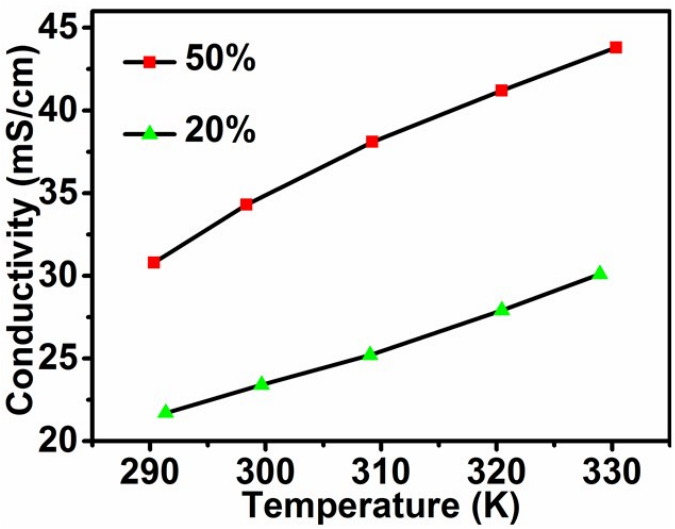

Figure S8. Temperature dependences of the conductivity of the PVEIm-Br aqueous solution, black squares (■) mean the conductivity of 50 wt% solution, green triangles (▲) are the conductivity of 20 wt% solution

Characterization of PIL-based humidity sensor:

The morphology of PIL-based humidity sensor was examined by field-emission scanning electron microscopy (SEM, ZEISS SUPRA 55).

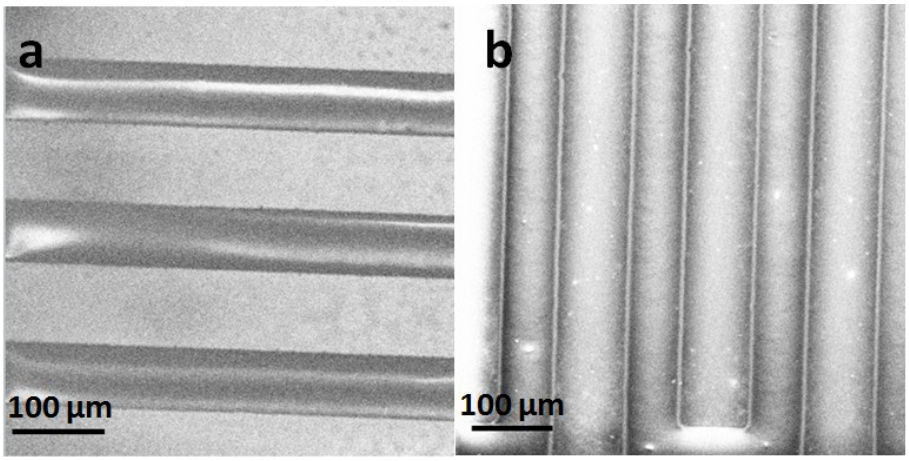

Figure S9. SEM images (top view) of (a) PVEIm-Br film and (b) PVEIm-BF_4 film.

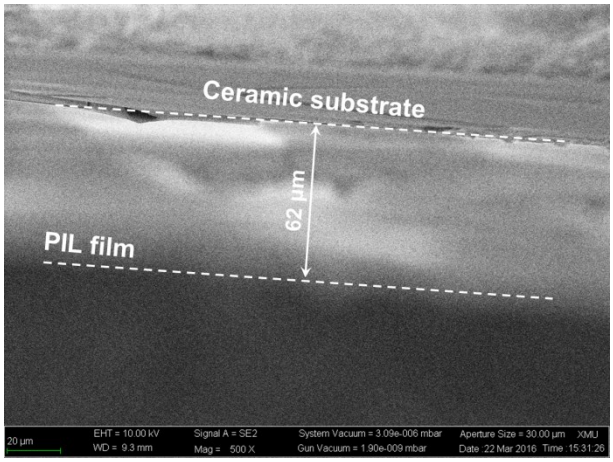

Figure S10. SEM images (side view) of PEVIm-Br film. The thickness of PEVIm-Br is approximately 62 μm.

Results and Discussions

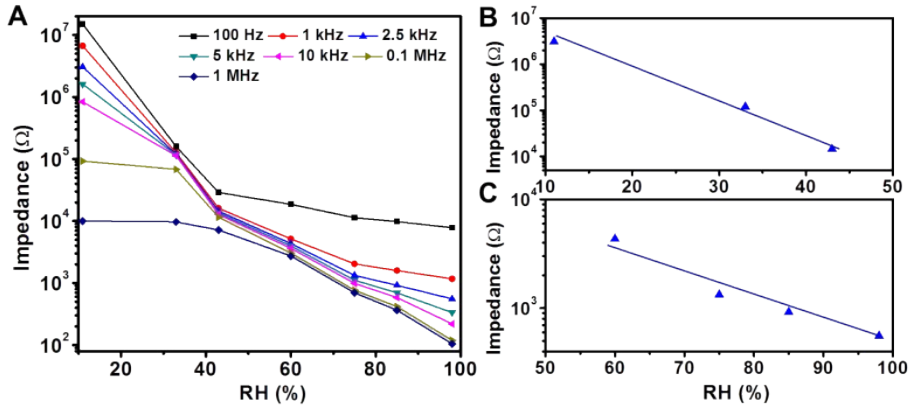

Figure S11. (A) The dependence of impedance on RH for PEVIm-Br sensors measured at various frequencies; (B) and (C) The linear ranges of the calibration curve obtained at 2.5 kHz.

The working frequency plays an important role in the humidity properties, thus the impedance as a function of RH at different frequencies were measured to determine the optimum frequency. As can be seen from Figure 1, the impedance of PEVImBr is greatly dependant on frequency at low relative humidity range (<43% RH), the impedance decreases with increasing frequency. However, at high relative humidity range (>43% RH), the effect of frequency on impedance is weak compared with that at low relative humidity range, indicating the dominance of two different sensing mechanisms. The best sensitivity of the impedance versus RH curve appeared at 2.5 kHz, with the impedance modulus varies from 3.23 MΩ to 670 Ω (approximately 4821-fold variation) as the relative humidity

changes from 11% to 98% RH. Thus 2.5 kHz could be defined as the ideal working frequency of the humidity sensor and used in the following measurements.

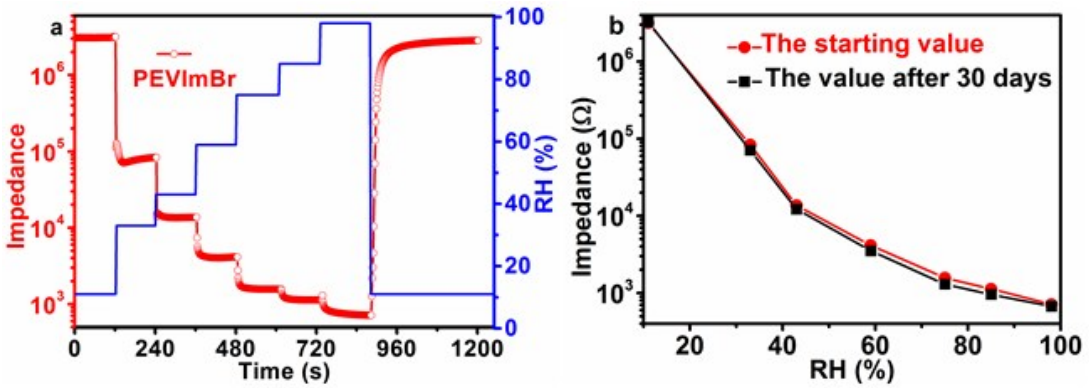

Figure S12. (a) The impedance modulus of the PEVIm-Br sensor vs. time in different relative humidity measured at 2.5 kHz, the sensor is stored without packaging for 30 days. (b) The comparison diagram of impedance modulus of the sensor in different relative humidity，black squares (■) mean the starting value, red spheres (●) are the value after 30 days.

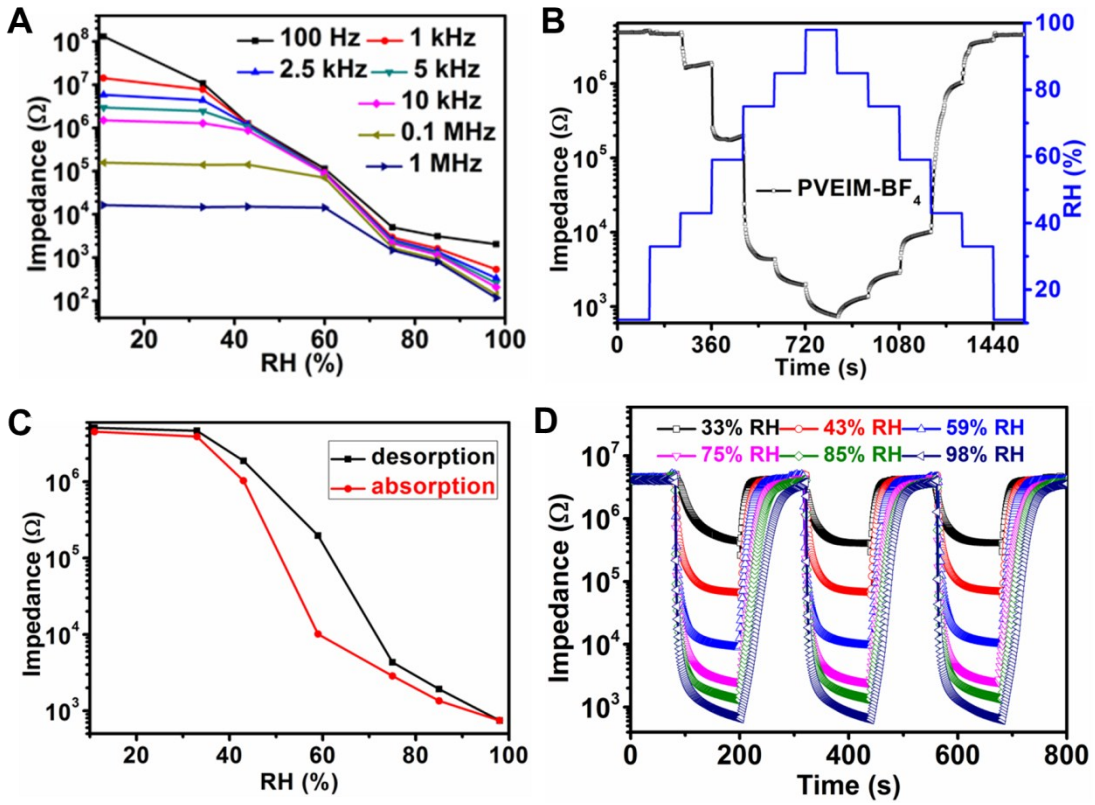

Figure S13. (A) The dependence of impedance on RH for PEVIm-BF_4 sensors measured at various frequencies; (B) Real-time frequency response of the sensor as the RH increased from 11% to 98% RH and returned to initial state; (C) The humidity hysteresis and (D) response and recovery properties of the PVEImBF_4-based sensors.

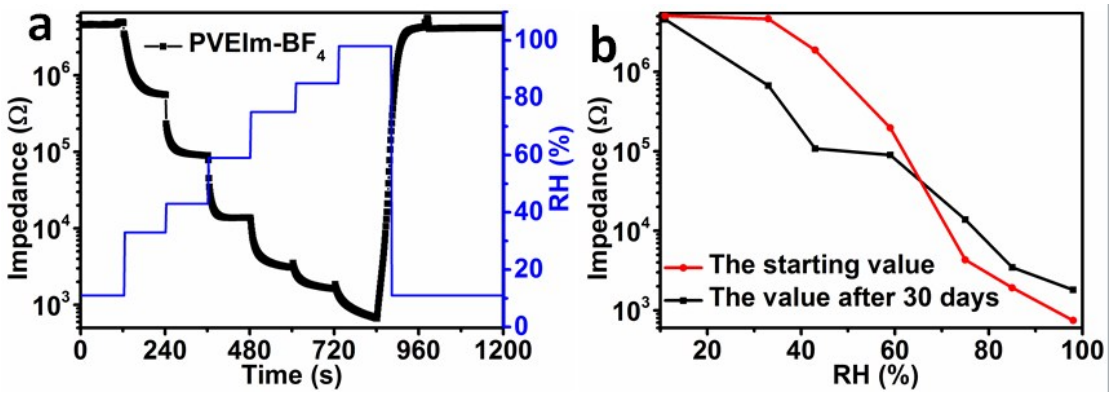

Figure S14. (a) The impedance modulus of the PEVImBF_4-based sensor vs. time in different relative humidity measured at 2.5 kHz, the sensor is stored without packaging for 30 days. (b) The comparison diagram of impedance modulus of the sensor in different relative humidity，black squares (■) mean the starting value, red spheres (●) are the value after 30 days.

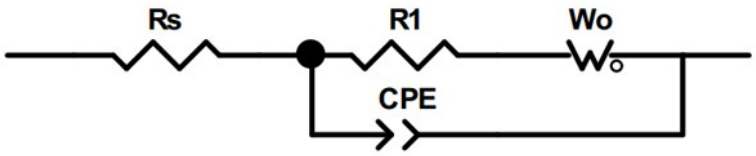

Figure S15. Equivalent electrical circuit of PIL-based humidity sensor.

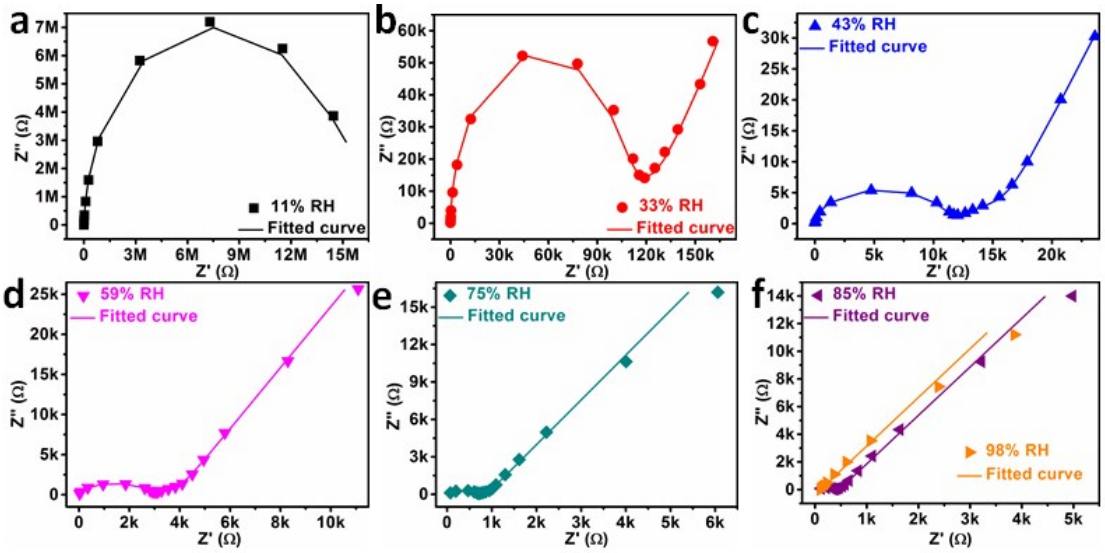

Figure S16. Nyquist plots of PEVIm-Br humidity sensor at different RH, points represent measured data, and solid lines represent simulated value using the equivalent circuit.

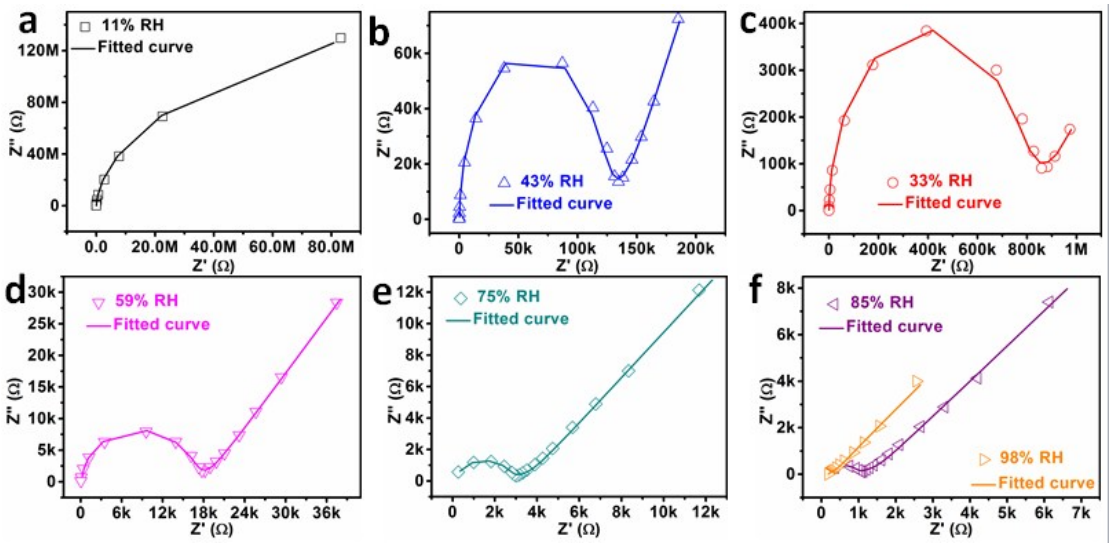

Figure S17. Nyquist plots of PEVIm-BF_4 humidity sensor at different RH, points represent measured data, and solid lines represent simulated value using the equivalent circuit.

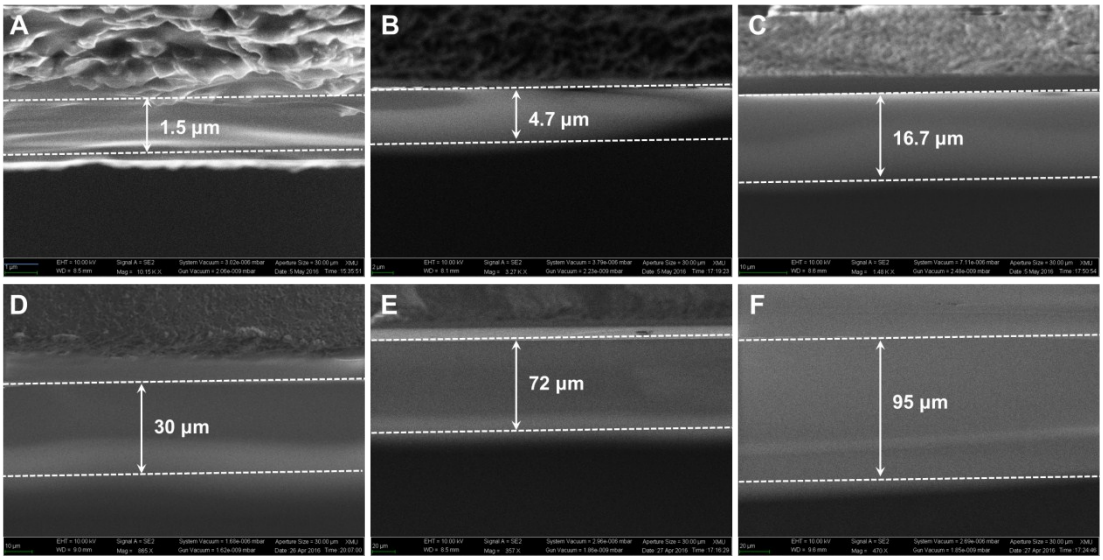

Figure S18. SEM images (side view) of PEVIm-Br film with different thickness.

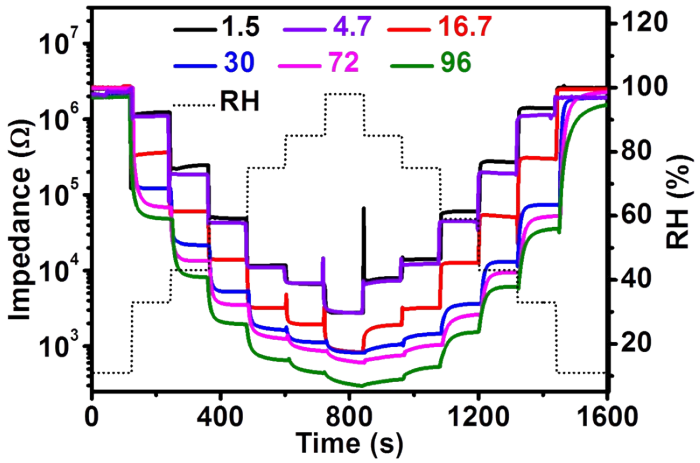

Figure S19. Comparison of the humidity–resistance characteristics of the PIL sensor with different thickness.

In order to investigate the correlation between PIL thickness and humidity sensor sensitivity, six samples with different thickness were prepared by adjusting spin-coating conditions including solution concentration and revolving speed (Figure S18). Figure S19 shows a comparison of the humidity–resistance characteristics of the PIL sensor with different thickness. We found that the PIL film thickness had an obvious effect on the sensitivity of humidity sensor: the sensitivity of PIL sensor increases with an increase in thickness. It is can be understood that thick-film sensor has a higher sensitivity, because the sensing mechanism of PIL humidity sensors is based on water

adsorption on the PIL surface, and the thick PIL film is more easier to form integral and continuous adsorbed water layer, which benefits for Grottus proton transfer, resulting in an increase in conductivity. However, the thick PIL films exhibit relative long response and recovery time compared with thin films, this is due to the fact that the water adsorption and desorption in thin-film sensors takes place only on the film surface, which requires less time for water adsorption/desorption. Considering the above factors, the optimal thickness of PIL film sensor should be 20~80 μm.

Table S2. Parameters of the equivalent circuit components

RH	**Component parameters**							
(%)	R_s (Ω)		R_1(Ω)		Z_{CPE}(Ω)		Z_w(Ω)	
	Br	BF_4	Br	BF_4	Br	BF_4	Br	BF_4
11	35.17	180	8.3698E6	4.5716E7	1.3888E7	1.1755E7	1.8412E6	1.0363E7
33	34.82	178.2	98759	727820	1.0189E7	9.6336E6	97927	479800
43	35.08	181.3	10643	114030	9.6544E6	8.4883E6	18284	115090
59	35.39	181.1	2683	15471	9.2506E6	7.9379E6	7117.6	21877
75	35.28	179.3	604.2	2355	8.8472E6	6.6592E6	2107.2	8285.8
85	36.02	179.5	279.3	687.9	8.209E6	4.8597E6	1335.4	4494
98	35.82	177	65.32	465.9	3.6719E6	4.5667E6	16.0748	2547.1

Table S3. Performance of the presented PIL sensors in this work compared with previous work

Sensor type	Sensing material	Working range (%RH)	Order of magnitude change	Hysteresis RH (%)	Response time (s)	Recovery time (s)	Ref
Resistive	PEVIm-Br	11-98	3	1	6	31	This work
Resistive	PEVIm-BF_4	11-98	3	10	31	59	This work
Resistive	PDEAEMA-b-PS	22-95	3	8	60	260	4
Resistive	QC-P4VP/RGO	15-90	3	4.5	21	78	5
Resistive	carbon spheres/PVA	9-97	3	--	19	178	6

Resistive	QC-P4VP/Ag	11-98	3	5	24	145	7
Resistive	rGO	30-90	3	2.5	28	48	8
Capacitive	PVP/PVA	11-98	2	--	37	10	9
Resistive	MWCNTs/ PAA	30-90	1	--	670	380	10
Resistive	PMMA/ PMAPTAC	10-90	2	6.1	45	150	11

References:

1. J. Yuan, C. Giordano and M. Antonietti, *Chemistry of Materials,* 2010, **22,** 5003-5012.

2. D. Gendron, A. Ansaldo, G. Bubak, L. Ceseracciub, G. Vamvounisc, D. Ricci, *Composites Science and Technology,* 2015, **117,** 364-370.

3. Y. Lin, F. Wang, Z. Zhang, J. Yang, Y. Wei, *Fuel,* 2014, **116,** 273-280.

4. W. Geng, X. He, Y. Su, J. Dang, J. Gu, W. Tian, Q. Zhang, *Sensors & Actuators B: Chemical*, 2015, **226**, 471-477.

5. Y. Li, K. Fan, H. Ban, M. Yang, *Sensors & Actuators: B Chemical*, 2016, **222**, 151-158.

6. B.B. Cunha, M.W.C.C. Greenshields, M.A. Mamo, N.J. Coville, L.A. Hümmelgen, *Journal of Materials Science Materials in Electronics*, 2015, **26**, 4198-4201.

7. Y. Li, T. Wu, M. Yang, *Materials Chemistry & Physics*, 2015, **153**, 346-352.

8. P. G. Su, C. F. Chiou, *Sensors & Actuators B: Chemical*, 2014, **200**, 9–18.

9. F. Teng, H. Zhao, J. Kai, X. Zhou, T. Zhang, *Journal of Applied Polymer Science,* 2013, **130**, 2056–2061.

10. J. Lee, D. Cho, Y. Jeong, *Solid-State Electronics*, 2013, **17**, 80-84.

11. P. G. Su, C. S. Wang, *Sensors & Actuators B: Chemical*, 2007, **123**, 1071-1076.